journal

J. Am. Ceram. Soc., 94 [6] 1893–1900 (2011)
DOI: 10.1111/j.1551-2916.2010.04295.x
© 2011 The American Ceramic Society

Grain Boundaries in Uranium Dioxide: Scanning Electron Microscopy Experiments and Atomistic Simulations

Pankaj V. Nerikar,[‡] Karin Rudman,[§] Tapan G. Desai,[¶] Darrin Byler,[‡] Cetin Unal,[‡] Kenneth J. McClellan,[‡] Simon R. Phillpot,[‖] Susan B. Sinnott,[‖] Pedro Peralta,[§] Blas P. Uberuaga,[‡] and Christopher R. Stanek[†,‡]

[‡]Los Alamos National Laboratory, Los Alamos, New Mexico 87545

[§]School of Mechanical, Aerospace, Chemical and Materials Engineering, Arizona State University, Tempe, Arizona 85287

[¶]Advanced Cooling Technologies Inc., Lancaster, Pennsylvania 17601

[‖]Department of Materials Science and Engineering, University of Florida, Gainesville, Florida 32611

The distribution and atomic structure of grain boundaries has been investigated in UO_2. Our scanning electron microscopic/electron backscatter diffraction experiments on a depleted UO_2 sample showed real nuclear fuels contain a combination of special coincident site lattice (CSL) and general boundaries. The experimental data indicated that ~16% of the boundaries were CSL boundaries and the CSL distribution was dominated by low Σ boundaries; namely Σ9, Σ3, and Σ5 Based on our experimental observations, the structures of select low Σ (Σ5 tilt, Σ5 twist, Σ3 tilt) and a random boundary were analyzed in greater detail using empirical potential atomic-scale calculations. Our calculations indicate that the boundaries have very different structures and each CSL boundary had multiple minima on the γ-surface. The presence of a significant fraction of CSL boundaries and the differences in their structures are expected to have important consequences on fuel properties.

I. Introduction

GRAIN boundaries (GBs) are two-dimensional (2D) defects where crystalline grains of differing orientation meet.[1] The atomic structure at GBs is typically very different than in the bulk. GBs in polycrystalline materials can typically be classified in two broad categories: low Σ boundaries (where Σ is the reciprocal density of coincident site according to the coincident site lattice (CSL) model[2]) and general GBs. Previous studies have shown that low Σ boundaries may exhibit interesting mechanical and kinetic properties such as high resistance to sliding, fracture and corrosion.[3] In the context of nuclear materials, GBs influence many of the material properties that govern fuel performance. For example, fission gas (FG) segregation is an important phenomenon for UO_2 nuclear fuel performance as the build up and release of that gas, as could be expected in an accident scenario, can lead to failure of the fuel rod. Because FGs such as xenon, which are insoluble in the fuel matrix, can migrate to and nucleate bubbles at GBs, GBs play an important role in bubble formation and subsequent release of FGs.[4] In order to determine the role of GBs on the materials properties that govern nuclear fuel performance (including FG transport), we must first understand the atomic scale structure of those GBs and their distribution within the fuel.

In this work, we present the results of complementary experimental and theoretical studies aimed at understanding GB structure in UO_2. The use of electron diffraction techniques allows for an assessment of GB character and distribution in polycrystalline materials. We have used scanning electron microscopy (SEM) and electron backscatter diffraction (EBSD) measurements to determine grain sizes, GB misorientation and the distribution of GBs in a depleted UO_2 sample. With these techniques, the character of the GB can be identified, but determining the atomic structure of the GB, necessary for understanding material properties such as FG segregation to GBs is not possible. Thus, we have used empirical potentials and density functional theory (DFT) to model the atomic structure of several boundaries shown to be present in UO_2 by the EBSD experiments. Specifically, we examined four different GBs: Σ3 tilt, Σ5 twist, Σ5 tilt, and an asymmetric disordered boundary.

Compared with metals, relatively little work has been done to characterize the atomic structure of GBs in fluorite structured materials that are isostructural to UO_2. Most studies have focused on yttria-stabilized zirconia (YSZ). For example, the Σ3 (111)/[110] tilt boundary, which is a highly symmetric twin boundary in face-centered cubic metals, has been studied both experimentally and through empirical potentials in YSZ by Shibata *et al.*[5] They observed good agreement between the experimental structure and that predicted by atomistic simulations. Fischer and Matsubara[6] investigated the structure and transport properties of Σ5 (310)/[001], Σ13 (320)/[001] tilt, and Σ5 (111) 60° twist GBs in YSZ using molecular dynamics (MD) simulations. The twist boundary was observed to have the smallest excess volume and the lowest formation energy. Dickey *et al.*[7] used a combination of *Z*-contrast scanning transmission electron microscopy and electron energy loss spectroscopy to examine the structures of Σ5 (310)/[001] and Σ13 (510)/[001] symmetric tilt GBs in YSZ. It was observed that the core structures were different from metals and were unique to fluorites. Both boundaries were observed to be composed of periodic arrays of symmetric structural units with a distinct unit for each boundary. Based on the experimental observations of Dickey and colleagues, Mao *et al.*[8] studied five different models of the symmetric Σ5 (310)/[001] tilt GB in cubic ZrO_2 using DFT. The calculated lowest energy structure, which included partially filled rows within the GB core, was observed to be in agreement with experimental observations.[7] Vonlanthen and Grobety[9] characterized grain misorientations and distribution of CSL GBs in cubic ZrO_2 using SEM-EBSD measurements. The total fraction of CSL GBs was found to be 17.8%.

Much less work has been done on establishing the atomic structures of GBs UO_2. Van Brutzel and Vincent-Aublant.[10]

I. Tanaka—contributing editor

Manuscript No. 28526. Received August 30, 2010; approved October 25, 2010.
[†]Author to whom correspondence should be addressed. e-mail: stanek@lanl.gov

studied the structural properties of several symmetrical tilt boundaries with misorientation angles ranging from 12.7° to 61.9°. They observed that for lower misorientation angles the GBs consisted of edge dislocations, while for higher misorientations, Schottky defects were dominant in the GB structure.

This paper is organized in the following manner: Section II describes the experimental and computational methodology used in this work, including the preparation and characterization of the UO_2 sample and the construction of models of the GBs for the atomistic calculations. Sections III and IV provide the results of experiments and simulations, respectively. Section V discusses the results of the previous sections. Section VI provides the conclusions.

II. Methods

(1) Experimental Procedure

Depleted UO_2 pellets 3 mm in diameter were fabricated with feedstock powder from ABB Atom[‡‡]. Powders were milled in a zirconia mill jar for 15 min in 15 g batches. Five of these batches were then combined and passed through a −60 mesh sieve. Individual pellets were produced using approximately 0.95 g of the resulting powder and pressed using a 6 mm die set at 40 MPa with a 60 s dwell. These green pellets were sintered at 1750°C for 10 h under flowing gas with a flow rate of 1 slpm. The sintering started with an initial heating ramp at 2°C/min and burnout with a 4-h hold at 450°C, followed by a ramp up to 800°C at 2°C/min all under dry Ar. Then, the gas was switched to Ar-6% H_2 bubbled through a water bath for the remainder of the run. Once the gas was switched to Ar-6% H_2, the temperature was ramped from 800° to 1750°C at 5°C/min followed by a 10 h hold. The pellets were cooled down to 30°C at a rate of 5°C/min.

One of the sintered pellets was then mounted in epoxy and sectioned longitudinally. After sectioning, the sample was ground with SiC paper (320–1200 grit) with water as lubricant and then polished using the following sequence: 5 min with 3 μm diamond paste, 3 min with 1 μm diamond and 3 min with 0.25 diamond. Polypropylene glycol was used as a lubricant in all of these sectioning steps. Finally, the sample was rinsed with water and ultrasonically cleaned in isopropanol and dried with hot air. For ease of manipulation and imaging in the electron microscope, the sample was thermally etched to reveal the GBs and carbon coated with a Bal-tec coater using carbon thread.

The microstructure characterization was performed at Arizona State University using a SEM equipped with an EDAX-TSL OIM™ attachment, and the OIM™ 5.31 analysis software. Secondary electron images of the sample were obtained initially to select a region of interest and to determine grain size and porosity distribution. EBSD data were then collected on this region with a step size of 0.2 μm to determine GB misorientations. The best results were obtained at 20 kV and 4 s exposure time (due to the carbon coating). Data points chosen for the analysis were such that they all had >95% probability of being indexed correctly, as estimated by the EDAX-TSL OIM™ analysis software. Furthermore, a minimum grain size of 10 pixels was used in the reconstruction of the microstructure from the crystallographic data to ensure that poorly indexed points at pores were not mistaken for individual grains during data analysis. Direct comparisons were made with optical and secondary electron images of the same region to ensure that the EBSD data resulted in maps that represented the actual microstructure.

Misorientation data were also collected manually at each GB to determine the number fraction of special boundaries. Misorientation data for 331 GBs were obtained and 53 of them were special GBs from the point of view that they corresponded to a CSL boundary within a tolerance determined by the Brandon criterion ($\Delta\theta = \theta_0/\Sigma^n$, $\theta_0 = 15°$, $n = 0.5$).[11] The analysis was conducted for CSLs up to Σ49. In addition, the analysis software was used to obtain the length fraction of each boundary type, i.e., the length of a boundary with a particular misorientation divided by the total GB length measured in the sample. Results on GB characteristics are reported here in terms of length fraction.

Finally, grains that formed selected low-Σ boundaries (3, 5, and 9) were analyzed using the EDAX-TSL software to obtain the crystallographic directions in each grain parallel to the average GB trace, for boundaries with fairly straight traces, or the directions parallel to long straight segments for those boundaries where the traces kinked at one or more locations. Once traces were obtained, they were used to find out how many of them were consistent with the standard GB planes for symmetric CSL boundaries, either tilt or twist, by taking the dot product of the trace with the normals to the twinning planes and with the rotation axes listed in the literature for each of these CSL GBs.[12] This was done as a first step to quantify the crystallography of the boundary planes and the nature of the boundary itself, i.e., tilt, twist, or mixed. If the GB trace vectors and the normals of the selected GB planes were not orthogonal for both grains, then they were considered mixed GBs.[13]

(2) Computational Methods

The atomic structure and properties of four representative GBs (as determined by experimental analysis) was considered using empirical potentials. The use of these potentials, rather than higher-fidelity electronic-structure methods, was necessary due to the large system sizes required to adequately describe the GB structure (up to 10 000 atoms). We used the potential developed by Basak *et al.*,[14] comprised of a Buckingham term plus a Morse term. This potential has been shown to be one of the better potentials for describing UO_2, especially its defect properties.[15] However, recognizing the possible limitations of these potentials, especially in describing structures such as GB far from the fitting space, we used limited DFT calculations to validate our results. The DFT calculations were performed with the projector augmented-wave [16] method. We utilized the SP-GGA+U (spin-polarized generalized gradient approximation with the Hubbard U_{eff} correction)[17] with a U_{eff} (U–J) value of 3.96 eV to include the effect of the strong correlation of 5f electrons in uranium as implemented in the Vienna Ab-Initio Simulation Package.[18,19] For the DFT calculations, we used a cell containing 360 atoms for the structural optimization where the cell volume was kept constant and the atomic positions relaxed. The Brillouin zone sampling used a $1 \times 1 \times 1$ Monkhorst-Pack[20] k-point mesh and the cut-off energy for the plane waves was 400 eV. Previous work has shown that the combination of the above parameters yields results in good agreement with experiments for bulk and defect properties.[21]

Because of the ionic nature of the material and the difficulty of terminating the simulation cell with free surfaces, periodic boundary conditions were used, resulting in two GBs in each simulation cell. Four such simulation cells were constructed with different GB misorientations. Three CSL GBs were considered: the Σ3 (111)/[110] symmetric tilt, Σ5 (310)/[001] symmetric tilt, and Σ5 (001) $\theta = 36.7°$ symmetric twist. The initial ideal symmetric GB structures were constructed using the software GBstudio.[22] In addition to the five macroscopic degrees of freedom describing the GB misorientation and the normal to the GB plane, there are microscopic degrees of freedom describing the relative translation between the two grains that must be optimized. We constructed the γ-surface, the map of the energy of the GB as a function of the relative translation of the two grains, for each of the three CSL boundaries by shifting one grain with respect to another in the plane of the boundary and minimizing both the atomic structure and the strain in the direction perpendicular to the boundary. The grain sizes chosen were approximately 1.8, 3.5, and 2.2 nm, respectively, after a convergence of GB energy with grain size was achieved. We allowed for relaxation of strain in the dimension perpendicular to the GB plane.

[‡‡]Swedish subsidiary of the ABB group that supplies nuclear power plants and fuels; http://www.abb.se/

We note that there are yet other degrees of freedom that in principle should be considered to find the atomic structure that minimizes the free energy of the GB. For example, the number of atoms in the boundary plane can be varied. This can be done by removing stoichiometric or charge neutral groups of atoms, as described by Chua *et al.*,[23] or even individual ions, if charge transfer is allowed to prevent net charging of the boundary, effectively changing the composition at the boundary. In this study, we have focused on boundaries with the original CSL composition for convenience. However, this has limited the types of boundaries we can consider. For example, we have examined the structure of a Σ9 tilt boundary but found that if the original composition is maintained, the lowest energy structure is highly disordered. We expect that if we allowed the atomic composition to vary (adding or subtracting a certain number of atoms), we would find an ordered boundary structure, as von Alfthan *et al.*[24] found for Si. Future work will consider these effects.

In addition to the CSL GBs, we also considered an asymmetric (110)(100)/[100], highly disordered GB which was constructed such that one grain had (100) planes parallel to the simulation cell in all the three directions. This GB had a tilt angle of 45° which is close to the peak of the misorientation angle distribution. The grain size was approximately 3.9 nm. We obtained the GB structure by bringing two grains of equal size together and annealing them at 800 K with MD using the Basak potential. During this process, we ensured that a well-equilibrated GB with no external strain was obtained.

III. Experimental Results

The microstructure in the region of interest for the depleted UO_2 sample examined is shown in Fig. 1, which displays an inverse pole figure (IPF) map, superimposed over a SEM image of the microstructure. In the IPF map, the colors for each grain correspond to the crystallographic orientation in the grain parallel to the out-of-plane direction, as given by the standard stereographic triangle in the inset. Special GBs are highlighted with different colors depending on their Σ value. The sample had equiaxed grains with an average grain size of 6 ± 2 μm and porosity with an area fraction of approximately 14%, which is consistent with the large porosity expected in an insulator pellet. Large pores were located mostly near GBs and triple points, while small pores were present mainly inside large grains.

The number fraction of individual CSL GBs obtained from the misorientation data collected manually was compared with the length fraction statistics provided by the EDAX-TSL OIM™ software. There were some differences between the two sets of results, especially regarding the fraction of Σ3 and Σ5 GBs. We note from Fig. 1 that, in general, the total number of Σ5 GBs is lower than for Σ3 GBs; however, the Σ5 GBs tend to have longer lengths than Σ3 GBs, which would result in differences between number and length fractions for these GBs that are consistent with the results obtained in this study. That is, the number fraction overestimates the abundance of Σ3 GBs and underestimates the fraction of Σ5 GBs when compared with their length fractions. Hence, collecting data on just the number of GBs does not truly reflect their actual "abundance" in the microstructure, even in this case where grains are fairly equiaxed. Therefore, the statistics of GB characteristics presented here corresponds to length fraction and not the number fraction, because the former is a more appropriate metric to represent GB statistics than the latter, as suggested by Randle.[25]

The distribution of specific misorientation angles obtained is shown in Fig. 2. Three different measures are shown: a correlated distribution, calculated from grains that share a common boundary; an uncorrelated distribution, calculated from the overall grain orientation distribution; and a random distribution, which represents the Mackenzie distribution for a cubic crystal.[26] The correlated distribution is the actual distribution present in the sample as it is obtained from grains that share a GB. The uncorrelated distribution is calculated from the texture and in that sense is purely "geometric" in nature, i.e., grain orientations from the measured texture are sampled and placed adjacent to each other which in turn results in a potential GB misorientation distribution. The difference between the two measures points to the effects influencing the microstructure. If the correlated and uncorrelated distributions are similar, then the GBs themselves, say, their energies, do not play a significant role on the final misorientation distribution.

The correlated distribution presented a maximum at about 42°, which agrees with the maximum for the uncorrelated distribution, but the amplitude of the peak was higher for the former, indicating that there is a tendency for boundaries with misorientations close to this angle to be present in the material with a frequency higher than that expected from just random pairing of the existing grains in the area chosen for examination. Note that the uncorrelated distribution resembles the random distribution, which indicates that the sample had either a random or a fairly weak crystallographic texture. The total fraction of CSL boundaries was determined to be 15.7%, which is comparable to 17.8%, reported by Vonlanthen and Grobety[9] for YSZ, an oxide with the fluorite structure.

The length fraction of individual CSL boundaries, with the respect to the overall CSL population, is shown in Fig. 3. As can be observed, the largest fraction of CSL boundary type was Σ9, followed by Σ3 with smaller fractions of Σ5 and Σ11. The general CSL distribution is similar to the one presented by Vonlanthen and colleagues for YSZ but with a significantly larger fraction of Σ9 and a smaller fraction of Σ3, Σ5, and Σ11. This result indicates that sintered YSZ has a similar, but not identical CSL distribution to conventionally sintered UO_2. This compar-

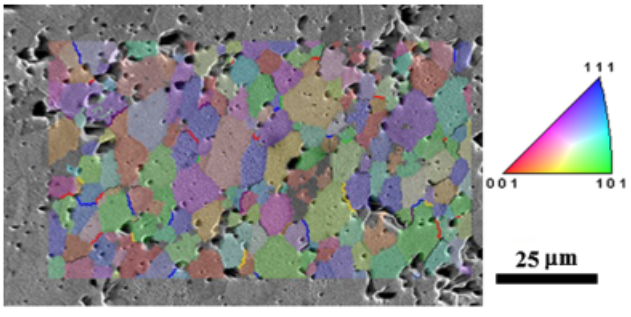

Fig. 1. SEM and EBSD images from the studied area of the depleted uranium oxide sample. The CSL GBs are highlighted in red (Σ3), yellow (Σ5), green (Σ7), blue (Σ9), purple (Σ11), and black (other special GBs). The scale bar is 25 μm long.

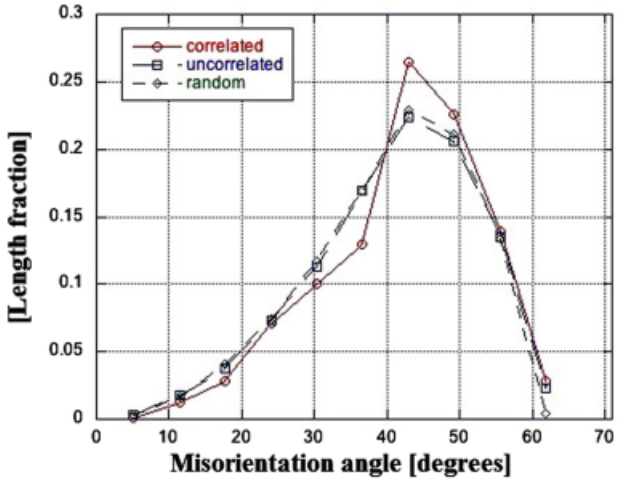

Fig. 2. Distribution of GB misorientation angle in the depleted uranium oxide sample. Open circles correspond to the correlated results, open squares are uncorrelated results and the open diamonds represent the Mackenzie distribution.

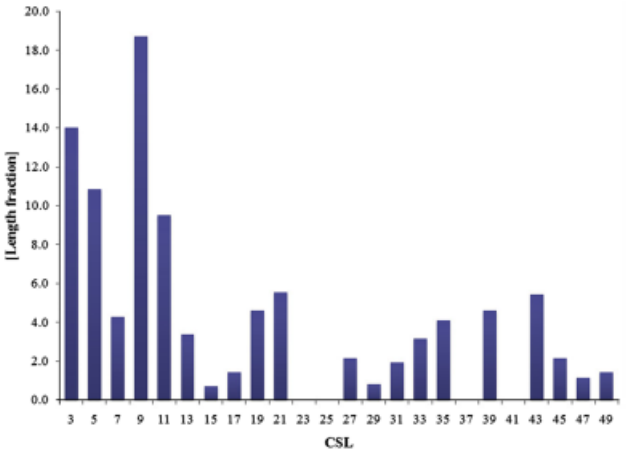

Fig. 3. CSL distribution for the depleted uranium oxide sample.

ison suggests that not all fluorite-structured compounds exhibit exactly the same GB misorientation distribution and/or that the final GB misorientation distribution depends to a significant degree on the processing conditions.

Regarding the analysis of the GB traces, there were cases where the GB traces in both grains were close to being perpendicular to more than one of the potential planes chosen, in that case, the GB plane that was closest to being 90° from the measured traces in the two grains was chosen. Traces and GB normals were typically within $<2°$ from being perpendicular to each other, well within the angular tolerance used to determine the CSL, i.e., Brandon[11] criterion, and also within the experimental error for the misorientation measurement, i.e., about 1°. The results are shown in Table I.

Most of the traces were consistent with either a twinning plane or a rotation axis except for the Σ5 GBs, which presented some mixed GBs. However, a full characterization to determine if the actual boundaries are pure twist or tilt requires five macroscopic degrees of freedom and cannot be achieved with 2D planar sections.[27] This will be the subject of further studies.

The results presented above indicate that low ΣGBs represent a significant fraction of the overall CSL distribution, about 44%. This is consistent with work published by Randle,[25] who established that for many materials and conditions, only a few types of special GBs dominate the Σ distribution. Therefore, in the following section, we consider the atomic structure of three different low ΣGBs (identified with SEM) as well as a disordered GB for comparison using atomistic modeling. It should be pointed out that the GB planes chosen were consistent with the trace analysis of Table I. These simulation results provide atomistic detail not possible with the experimental techniques used above.

Table I. Percentage of Boundaries Examined with Traces Consistent with High Symmetry Planes for a Subset of Σ3, Σ5, and Σ9 GBs

Sigma	Potential planes[12]	Percentage of GBs with consistent traces
3	{111}	91
	{211}	9
	Mixed	0
5	{100}	14
	{301}	57
	Mixed	29
9	{221}	33.3
	{411}	33.3
	{110}	33.3
	Mixed	0

GB, grain boundary.

IV. Computational Results

As discussed above, ~16% of the GBs experimentally observed in the UO_2 sample were CSL boundaries. As these experiments cannot probe the atomic structure of these boundaries (a crucial element for predicting e.g. segregation behavior to the boundaries), we have performed atomistic modeling of four representative boundaries: Σ5 twist, Σ3 tilt, Σ5 tilt, and an asymmetric disordered boundary. The initial structure, γ-surface and the lowest energy structure for the Σ5 twist boundary are shown in Figs. 4(a)–(c), respectively. The black dots in (b) are the initial 10×10 grid used for mapping out the γ-surface while the contours and colors represent the energies of relaxed structural minima of the boundary. The γ-surface is very complex, especially considering the relative simplicity of this GB, with many distinct local minima. The difference in energy between the lowest and the highest energy points was only ~0.14 J/m^2, which is not large compared with the other GBs considered later. The relaxed structures exhibit greater atomic displacements on the oxygen sublattice than on the uranium lattice, distorting the ring-like symmetry observed for the initial twist boundary (compare Figs. 4(a)–(c)). Fisher and Matsubara[6] studied the Σ5 twist boundary in YSZ using MD simulations. Similar to our observations for UO_2, they found that the disorder at the boundary was largely confined to the oxygen sublattice, though the distortion of the oxygen sublattice was greater in YSZ than what we observe for UO_2.

The initial structure, γ-surface and the lowest energy structure for the Σ3 (111)/[110] tilt boundary are shown in Figs. 5(a)–(c), respectively. The γ-surface is essentially featureless, indicating that there are only a few unique structures for this boundary. High-energy structures were only observed for translations with a zero component along the tilt axis. The initial structure (Fig. 5(a)) has mirror symmetry across the boundary, which is a common feature of all of the initial boundaries. For the lowest energy structure, the bulk *U–O* interatomic distance of ~2.37 Å was maintained even at the boundary, indicating that the (111) planes maintain the same spacing across the boundary. In the minimum energy structure of the γ-surface, illustrated in Fig. 5(c), the common mirror symmetry of both sublattices was broken.

Our calculated structure is quite similar to the one found by Shibata *et al.*[5] for YSZ using high-resolution transmission electron microscopy (HRTEM) and atomic simulations. As the position of the anion sublattice could not be confirmed solely by TEM, they performed a lattice statics study with empirical potentials, in which the translations were performed to find a minimum energy boundary structure. They found good agreement between the simulated and experimental TEM image. Our calculated structure also has separate mirror planes of symmetry (indicated by the dashed lines in Fig. 5(c)) for the anion and cation sublattices. Moreover, the anion sublattice distorted to a structure that minimized oxygen repulsion and was energetically favorable.

The Σ5 tilt (310)/[001] is perhaps the most studied boundary in fluorites due to its simple geometrical construction and the fact that it has been observed experimentally.[7] The initial CSL structure, the obtained γ-surface and the minimum energy structure are illustrated in Figs. 6(a)–(c), respectively. As with the Σ5 twist, there were multiple minima on the γ-surface, indicating that there are many different stable structures for this GB. Our calculations found a basin of low energy minima centered at the (0.5[100], 0.5[310]) translation vector. The high-energy local minima, including the original untranslated boundary of Fig. 6(a), were confined to translations along [310]. Comparing the untranslated ideal Σ5 tilt boundary structure with the lowest energy structure on the γ-surface (Figs. 6(a) and (c)), we found that the atomic structure of the higher energy configuration is fully symmetric across the GB plane, while that of the lowest energy GB exhibited a slight asymmetry arising from an a reconstruction of the anion sub lattice. This asymmetry is not related to the crystallographic asymmetry associated with GBs

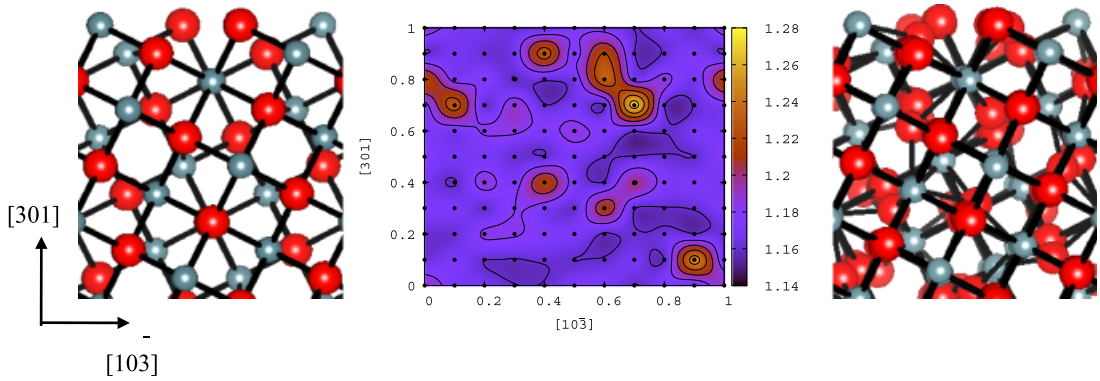

Fig. 4. Structure of Σ5 twist boundary: (a) initial structure, viewed from along (010), (b) γ-surface plot, and (c) translated and relaxed. The black dots in (b) are the initial 10x10 grid used for mapping the γ-surface while the colors in the contour plot represent the energy of relaxed local minimum structures of the boundary. Uranium ions are shown in smaller spheres and oxygen ions as bigger spheres.

in which the two grains have differing orientations. The nature and degree of this asymmetry depends delicately on the specific atomic interactions.[28]

Our lowest energy structure is different from that observed by Van Brutzel and Vincent-Aublant.[10] Their structure incorporated Schottky defects into the GB core to alleviate the strain at the boundary. In our structure, this strain is relieved by a greater reconstruction of the oxygen sublattice, forming a ring-like oxygen pattern. The different GB structure predicted by Van Brutzel and colleagues could also be explained by the use of a different empirical potential form. We have confirmed the sensitivity of GB structure on the empirical potential used by comparing our results using the Basak potential with another potential from Busker *et al.*,[29] which finds a different structure for the global minimum in the γ-surface. However, both the Basak and Busker potentials found structures located near the center of the γ-surface that were much lower in energy than the idealized (but relaxed) Σ5 GB. Moreover, both potentials exhibited a ridge of high-energy local minima along [310] translation direction. Thus, while the detailed structure differed, there were some commonalities between the predictions of the two potentials.

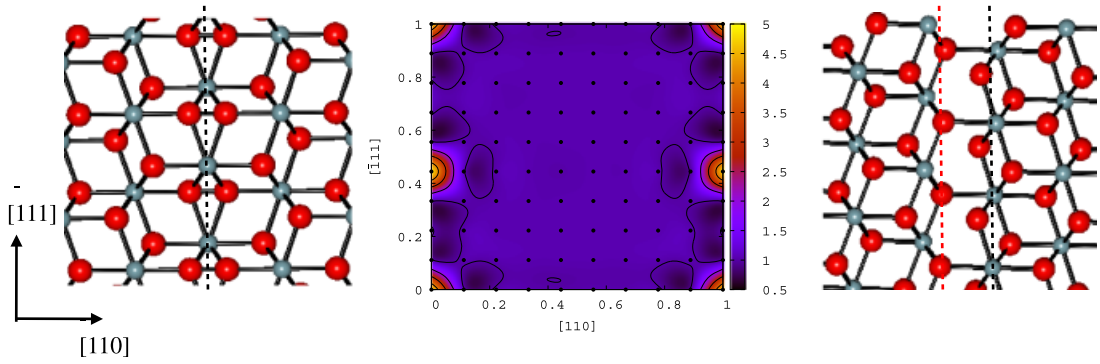

Fig. 5. Structure of Σ3 tilt boundary: (a) initial, (b) γ-surface plot, and (c) translated and relaxed. The dotted line in (a) represents the original grain-boundary plane. In the relaxed structure (c), the anion and cation sublattice have different mirror planes, as indicated by the dashed lines (red for anions, black for cations). The scheme is the same as used in Fig. 4.

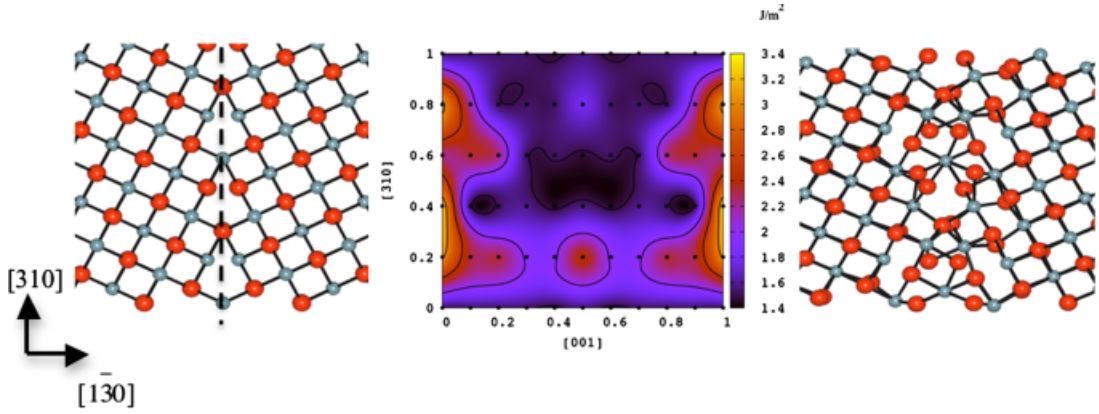

Fig. 6. Structure of the Σ5 tilt boundary using the Basak potential:a) idealized, (b) γ-surface plot, and (c) translated and relaxed. The scheme is the same as used in Fig. 4.

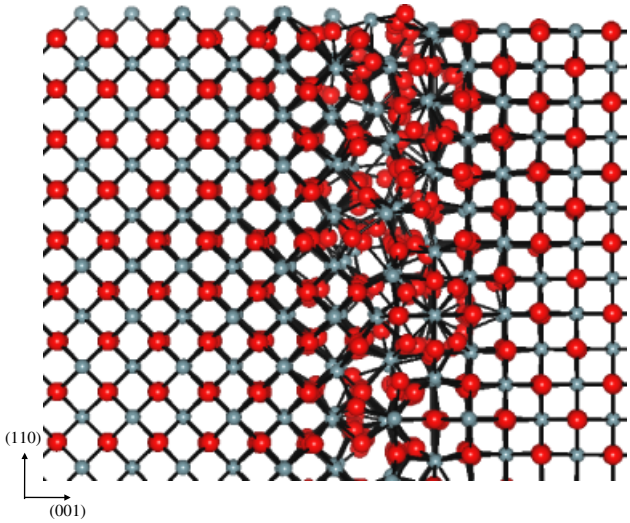

Fig. 7. Relaxed structure of the asymmetric (110)(100)/[100] tilt boundary highly disordered grain boundary.

Finally, as a significant number of the boundaries observed in the experimental analysis were not CSL boundaries, we also considered an asymmetric (110)(100)/[100] tilt boundary (Fig. 7) that is structurally different from the ideal tilt and twist boundaries. As discussed in Section II, we ensured that a well-equilibrated structure with no external strain was created. We also analyzed the structure to determine the bonding environment of uranium within the boundary compared with the grain interiors. The peaks in the uranium–uranium radial distribution function for both the grain interior and the GBs were at the same positions as in the ideal fluorite structure. However, the peaks for the GB were broader than the bulk, suggesting that while the uranium ions still maintain an overall bulk-like separation within the boundary, there are distortions within the GB structure. The uranium–oxygen bond distances at the two boundaries were slightly smaller (2.27 and 2.32 Å, respectively) than the 2.37 Å for the ideal fluorite structure. Moreover, a ring-like pattern was observed on one side of the boundary. This suggests that even though the boundary is "disordered," the oxygen sublattice is still attempting to order to the extent possible.

After the structures of the four different GBs were identified, we determined their relative stability. To do so, we calculated the GB energy, which is defined as the energy required to form a boundary, obtained from the usual equation:

$$E_{GB} = \frac{(E_{tot} - nE_{bulk})}{2A} \quad (1)$$

Here E_{tot} is the total energy of the supercell, E_{bulk} is the total energy of bulk UO_2 per formula unit, n is the total number of UO_2 formula units in the supercell, and A is the area of the GB plane. The factor of two accounts for the fact that there are two GBs in the supercell. The boundary energies are given in Table II. The calculations predict that the Σ3 tilt GB has the lowest energy. This is not surprising because, even at the boundary, the bulk interatomic distances are relatively well maintained; that is, it is the most "bulk-like" of the boundaries considered. Boundaries with low values of Σ, having a high density of coincident sites, are generally regarded as more stable boundaries. However, this is a necessary yet insufficient condition for stability as pointed out by Wolf.[30] Other factors such as the orientation of the grains are also important considerations. The highly disordered, asymmetric boundary had the highest boundary energy among the four boundaries considered. This is due to the fact that the three Σ boundaries have relatively little misfit on an atomic scale. Of the two Σ5 boundaries, the twist boundary was predicted to be lower in energy than the tilt, in agreement with the results of Fisher and Matsubara for YSZ.

Table II. Grain-Boundary Energies of All Four Boundaries Calculated Using the Basak Potential

Boundary type	Grain boundary energy (J/m^2)
Σ3 tilt	1.04
Σ5 twist	1.17
Σ5 tilt	1.58
Asymmetric	1.86

It has been argued[31] that the GB energy can be related to the segregation energy, defined as the difference in energy of a solute at the boundary as compared with the bulk. Boundaries with low interfacial energies can be expected to have low segregation energies (for the same size of the solute), because, in absence of other factors, they have smaller volume expansion and hence a lower propensity toward impurity segregation. Based on this result, we expect the asymmetric GB to have the highest segregation energy. This will be discussed in greater detail in future paper.

V. Discussion

The fact that our EBSD measurements showed a large fraction of Σ boundaries to be present in UO_2 encouraged us to examine their structure in greater detail with atomistic simulations. Their concentration is significant enough to influence materials properties, for example, the segregation of FG to GBs. Looking at Σ3, 5 and 9 as well as the random boundary (as a representative of the most common misorientation angle non-CSL GBs) gives an overall view of the typical boundaries in the material and allows us to make deductions about their effects on bulk material behavior.

It is useful to compare and contrast some of the details of the experimental observations and the simulation results. The experiments showed that the Σ9 boundary is the abundant CSL boundary in the sample considered (18% of all CSL boundaries). This seems to suggest that experimentally, the microstructure is kinetically trapped in some metastable state. This is because thermodynamically the Σ3 boundary would have been the most abundant because it is the most "bulk-like" and highly symmetric of all the Σ boundaries and thus has the lowest GB energy. In fact, all GBs are metastable to some degree and their presence is an indication that thermodynamic equilibrium has not been achieved. It is quite probable that further annealing and grain growth may change the GB distribution observed in our experiments.

In addition to the metastability in the form of kinetic trapping of different GBs, there is another type of metastability observed for each particular GB type. For each CSL boundary considered here, there are multiple structures that often have rather similar energies. Thus, there is not one unique structure for even the simplest of these boundaries. These local minima may influence the actual structure of the boundary and consequently the properties of the material.[32]

We note that calculating the γ-surface is just one of the ways of finding a low energy structure. Indeed this was observed when the lowest energy structure for the Σ5 tilt boundary was annealed at high temperature. The annealing resulted in a structure which was 0.16 J/m^2 lower in energy than lowest energy structure at 0 K. At least for this boundary, this difference is small compared with the range of structures in the γ-surface ($\sim$2.0 J/m^2) and we expect the qualitative trends in physical properties to be unaffected by the choice of the lowest energy structure on the γ-surface as our model Σ5 tilt boundary.

Given the complexity in identifying the lowest energy atomic structure for a given GB and the fact that empirical potentials used were derived from bulk properties, it was important to test

the suitability of these potentials for GB calculations. Therefore, we considered the initial Σ5 tilt structure and the lowest energy structure predicted by the Basak potential as input to SP-GGA+U calculations. The relaxed DFT structure of this boundary was very similar to that found with the Basak potential; no atom moved by >0.17 Å between the two methods. Thus, DFT validated the local oxygen rearrangements predicted by the Basak potential. However, we note that DFT found the fully symmetric GB structure to be lower in energy than the reconstructed asymmetric structure by 0.14 J/m^2. Moreover, it is generally assumed that near the GB there will be charge transfer from the cations to the anions to reduce electrostatic repulsion between like charged ions.[33] However, in the DFT calculations, the maximum charge transfer observed compared with the bulk was only 0.5% (calculated using the magnetic moments). Further analysis showed a maximum difference of Bader atomic charge[34] of 0.1e for uranium atoms at the boundary, indicating negligible charge transfer. Both of these observations instill confidence that the potentials capture GB phenomena reasonably well, at least from the point of view of describing charge transfer, or the lack thereof. Further, any discrepancies between the potentials and DFT are not a consequence of the fixed charge assumption of the potentials, but rather the chemical interaction between the atoms. Moreover, our predicted structure for the Σ3 tilt GB matches the experimentally observed structure of Shibata *et al.*[5] Finally, in our previous study on Σ5 tilt GBs in fluorites using empirical potentials,[28] we were able to reproduce the experimentally observed cation lattice structure in cubic ZrO_2. Such validations culminate in a compelling case for the use of empirical potentials in capturing the general physical trends of GB in UO_2.

Still, it is possible to improve the connection between modeling and experiment, enabling more quantitative comparison between the two. For example, on the simulation side, approaches, such as removing atoms at the boundary[23] may yield even more stable GB structures. Targeted experiments can be carried out to quantify the effect of processing conditions (temperature, annealing time) on the GB misorientation distribution. In addition, serial sectioning of the sample would help us distinguish between tilt and twist boundaries. Five parameters are needed to fully describe a GB, three that describe the lattice misorientation (angle/axis pair) and two for the boundary plane normal. The first three parameters can be derived from the EBSD data. However, data from serial sectioning of the samples would provide the 3D information needed to obtain the complete GB geometry and determine the boundary plane normal. Also, with aberration corrected HRTEM, we may be able to resolve the atomic structure of the GB, though imaging the oxygen sublattice may still prove challenging. Such TEM studies have recently revealed the atomic structure of dislocation cores in Al_2O_3.[35]

VI. Conclusions

We have presented a different approach to examine GB in UO_2, using SEM/EBSD measurements to identify relevant GBs, the structures of which can be considered in more detail with atomistic simulations. The aim of this work was to improve our understanding of structure of GBs in UO_2, both in terms of their distribution within a real material and their structure on the atomic level. EBSD measurements on a depleted UO_2 sample showed that $\sim$16% of the boundaries were CSL boundaries. Of these special boundaries, a higher concentration of Σ9 CSL GBs were observed than Σ3, Σ5, and Σ11. The fact that there was a higher concentration ofΣ9 GBs was attributed to the microstructure evolution being limited by kinetic processes.

Based on the experimental observations, the structures of select low Σ GBs (Σ5 tilt, Σ5 twist, Σ3 tilt) were analyzed in greater detail using empirical potential atomic-scale calculations. An asymmetric, highly disordered GB (representative of both the most common and non-CSL GBs) was also examined in the same fashion. The γ-surface was calculated to determine the minimum energy structures for each of the three Σ boundaries. For the Σ5 twist and Σ5 tilt boundaries, we observed multiple low energy minima, whereas the γ-surface for the Σ3 tilt boundary was essentially featureless. The lowest energy GB structure predicted for the Σ3 tilt boundary was a highly symmetric twin GB structure while for Σ5 tilt boundary, the predicted lowest energy structure exhibited a slight asymmetry on either side of the boundary plane. In all cases, idealized structures were found to be higher in energy than the minimum energy structures found upon minimizing the translational degrees of freedom. The Σ3 tilt boundary was observed to have the lowest GB energy among the four boundaries considered.

Our combined experimental and atomistic studies results showed that real nuclear fuel materials contain a combination of both special CSL boundaries and random non-CSL boundaries. Further, though not a surprise, these boundaries have very different structures and are expected to play very different roles in how they interact with both other boundaries and FG within the material. More surprisingly, even the simplest of these boundaries had multiple atomic structures that were close in energy. From the perspective of predicting fuel properties within a mesoscale model, it will be necessary to account for both this actual distribution of GBs as well as the differences in their properties. Our focus is to observe how much the differences in the atomic details matter at the mesoscale level to influence fuel properties. Future work will examine these effects in greater detail.

Acknowledgments

Computational work at LANL was sponsored by the Nuclear Energy Advanced Modeling and Simulation (NEAMS) program. P. V. N. also acknowledges support from the Seaborg Institute at Los Alamos National Laboratory. Los Alamos National Laboratory, an affirmative action/equal opportunity employer, is operated by Los Alamos National Security, LLC, for the National Nuclear Security Administration of the U.S. Department of Energy under contract DE-AC52-06NA25396. SBS and SRP gratefully acknowledge support from DMR-0426870. Work at ASU was supported by Department of Energy under agreement # DE-AC52-06NA25396 with Los Alamos National Laboratory and agreement # DE-NE0000134 001 with the Office of Nuclear Energy.

References

[1]S. M. Allen and E. L. Thomas, *The Structure of Materials*. John Wiley & Sons, New York, 1999.
[2]A. Brokman and R. W. Balluffi, "Coincident Lattice Model for the Structure and Energy of Grain Boundaries," *Acta Metall.*, **29**, 1703–19 (1981).
[3]G. Palumbo, E. M. Lehockey, and P. Lin, "Applications for Grain Boundary Engineered Materials," *JOM—J. Miner. Met. Mater. Soc.*, **50**, 40–3 (1998).
[4]D. R. Olander and P. Van Uffelen, "On the Role of Grain Boundary Diffusion in Fission Gas Release," *J. Nucl. Mater.*, **288**, 137–47 (2001).
[5]N. Shibata, F. Oba, T. Yamamoto, Y. Ikuhara, and T. Sakuma, "Atomic Structure and Solute Segregation of a Σ = 3, [110]/{111} Grain Boundary in an Yttria-Stabilized Cubic Zirconia Bicrystal," *Philos. Mag. Lett.*, **82**, 393–400 (2002).
[6]C. A. J. Fisher and H. Matsubara, "The Influence of Grain Boundary Misorientation on Ionic Conductivity in YSZ," *Appl. Phys. Lett.*, **19**, 703–7 (1999).
[7]E. C. Dickey, X. D. Fan, and S. J. Pennycook, "Structure and Chemistry of Yttria-Stabilized Cubic-Zirconia Symmetric Tilt Grain Boundaries," *J. Am. Ceram. Soc.*, **84**, 1361–8 (2001).
[8]Z. G. Mao, S. B. Sinnott, and E. C. Dickey, "Ab Initio Calculations of Pristine and Doped Zirconia 5 (310)/[001] Tilt Grain Boundaries," *J. Am. Ceram. Soc.*, **85**, 1594–600 (2002).
[9]P. Vonlanthen and B. Grobety, "CSL Grain Boundary Distribution in Alumina and Zirconia Ceramics," *Ceram. Int.*, **34**, 1459–72 (2008).
[10]L. Van Brutzel and E. Vincent-Aublant, "Grain Boundary Influence on Displacement Cascades in UO_2: A Molecular Dynamics Study," *J. Nucl. Mater.*, **377**, 522–7 (2008).
[11]D. G. Brandon, "Structure of High-Angle Grain Boundaries," *Acta Metall. Mater.*, **14**, 1479 (1966).
[12]H. Mykura, *Checklist of Cubic Coincidence Site Lattice Relations. Grain-Boundary Structure and Kinetics*. American Society for Metals, Metals Park, 1979.
[13]D. Wolf, *Handbook of materials modeling*, Vol. 2. Springer, New York, 2005.
[14]C. B. Basak, A. K. Sengupta, and H. S. Kamath, "Classical Molecular Dynamics Simulation of UO_2 to Predict Thermophysical Properties," *J. Alloys Compd.*, **360**, 210–6 (2003).
[15]K. Govers, S. Lemehov, M. Hou, and M. Verwerft, "Comparison of Interatomic Potentials for UO_2. Part I: Static Calculations," *J. Nucl. Mater.*, **366**, 161–77 (2007).

[16]P. E. Blöchl, "Projector Augmented-Wave Method," *Phys. Rev. B*, **50**, 17953–79 (1994).
[17]S. L. Dudarev, D. N. Manh, and A. P. Sutton, "Effect of Mott-Hubbard Correlations on the Electronic Structure and Structural Stability of Uranium Dioxide," *Philos. Mag. B.*, **75**, 613–28 (1997).
[18]G. Kresse and J. Furthmüller, "Efficient Iterative Schemes for Ab Initio Total-Energy Calculations Using a Plane-Wave Bases Set," *Phys. Rev. B*, **54**, 11169–86 (1996).
[19]G. Kresse and J. Hafner, "Abinitio Molecular-Dynamics for Liquid-Metals," *Phys. Rev. B*, **47**, 558–61 (1993).
[20]H. J. Monkhorst and J. D. Pack, "Special Points for Brillouin-Zone Integrations," *Phys. Rev. B*, **13**, 5188–92 (1976).
[21]P. Nerikar, T. Watanabe, J. Tulenko, S. Phillpot, and S. Sinnott, "Energetics of Intrinsic Point Defects in Uranium Dioxide from Electronic-Structure Calculations," *J. Nucl. Mater.*, **384**, 61–9 (2009).
[22]H. Ogawa, "GBstudio: A Builder Software on Periodic Models of CSL Boundaries for Molecular Simulation," *Mater. Trans.*, **47**, 2706–10 (2006).
[23]A. L. S. Chua, N. A. Benedek, L. Chen, M. W. Finnis, and A. P. Sutton, "A Genetic Algorithm for Predicting the Structures of Interfaces in Multicomponent Systems," *Nat. Mater.*, **9**, 418–22 (2010).
[24]S.von Alfthan, P. D. Haynes, K. Kaski, and A. P. Sutton, "Are the Structures of Twist Grain Boundaries in Silicon Ordered at 0 K," *Phys. Rev. Lett.*, **96**, 055505, 4pp, (2006).
[25]V. Randle, "Sigma-Boundary Statistics by Length and Number," *Interface Sci.*, **10**, 271–7 (2002).
[26]J. K. Mackenzie, "2nd Paper on Statistics Associated with the Random Disorientation of Cubes," *Biometrika*, **45**, 229–40 (1958).
[27]V. Randle, "Application of Electron Backscatter Diffraction to Grain Boundary Characterisation," *Int. Mater. Rev.*, **49**, 1–11 (2004).
[28]P. V. Nerikar, C. R. Stanek, S. R. Phillpot, S. B. Sinnott, and B. P. Uberuaga, "Intrinsic Electric Fields in Nanostructured Ceramics," *Phys. Rev. B*, **81**, 064111, 7pp, (2010).
[29]G. Busker, R. W. Grimes, and M. R. Bradford, "The Solution and Diffusion of Ruthenium in $UO_{2\pm x}$," *J. Nucl. Mater.*, **312**, 156–62 (2003).
[30]D. Wolf, "Properties of High-Angle (001) Twist Grain-Boundaries in Alkali-Halide Bicrystals—A Theoretical Investigation," *Philos. Mag. A*, **49**, 823–44 (1984).
[31]K. L. Merkle and D. Wolf, "Correlations between Grain-Boundary Structure and Energy," *Mater. Res. Soc. Symp. P*, **229**, 185–90 (1991), 359.
[32]D. Farkas, "Atomistic Theory and Computer Simulation of Grain Boundary Structure and Diffusion," *J. Phys.: Condes. Matter*, **12**, R497–516 (2000).
[33]J. H. Harding and C. Noguera, "Empirical and Ab Initio Local-Density Approximation Studies of an MgO(100) Twist Grain Boundary," *Philos. Mag. Lett.*, **77**, 315–20 (1998).
[34]W. Tang, E. Sanville, and G. Henkelman, "A Grid-Based Bader Analysis Algorithm without Lattice Bias," *J. Phys.-Condens. Mater.*, **21**, 084204, 7pp, (2009).
[35]N. Shibata, M. F. Chisholm, A. Nakamura, S. J. Pennycook, T. Yamamoto, and Y. Ikuhara, "Nonstoichiometric Dislocation Cores in Alpha-Alumina," *Science*, **316**, 82–5 (2007). □